Experimental Quantum Principal Component Analysis via Parametrized Quantum Circuits

Tao Xin,[1,2,*] Liangyu Che,[1] Cheng Xi,[1] Amandeep Singh,[1] Xinfang Nie,[1] Jun Li,[1,2,†] Ying Dong,[3,‡] and Dawei Lu[1,2,§]

[1]*Shenzhen Institute for Quantum Science and Engineering and Department of Physics, Southern University of Science and Technology, Shenzhen 518055, China*
[2]*Guangdong Provincial Key Laboratory of Quantum Science and Engineering, Southern University of Science and Technology, Shenzhen 518055, China*
[3]*Research Center for Quantum Sensing, Zhejiang Lab, Hangzhou, Zhejiang, 311121, China*

(Received 23 June 2020; revised 20 November 2020; accepted 23 February 2021; published 18 March 2021)

Principal component analysis (PCA) is a widely applied but rather time-consuming tool in machine learning techniques. In 2014, Lloyd, Mohseni, and Rebentrost proposed a quantum PCA (qPCA) algorithm [Lloyd, Mohseni, and Rebentrost, Nat. Phys. **10**, 631 (2014)] that still lacks experimental demonstration due to the experimental challenges in preparing multiple quantum state copies and implementing quantum phase estimations. Here, we propose a new qPCA algorithm using the hybrid classical-quantum control, where parameterized quantum circuits are optimized with simple measurement observables, which significantly reduces the experimental complexity. As one important PCA application, we implement a human face recognition process using the images from the Yale Face Dataset. By training our quantum processor, the eigenface information in the training dataset is encoded into the parameterized quantum circuit, and the quantum processor learns to recognize new face images from the test dataset with high fidelities. Our work paves a new avenue toward the study of qPCA applications in theory and experiment.

DOI: 10.1103/PhysRevLett.126.110502

Introduction.—The past decade has witnessed rapid progress in machine learning and quantum information science and in particular their preliminary amalgamation [1–5]. Machine learning techniques have been widely employed as powerful tools in pattern recognition, statistical analysis, and optimization. Besides being enhanced by increasing the classical computing power, machine learning can also be boosted with the aid of quantum computers, yielding a quantum speedup [6–10]. The quantum machine learning has been explored algorithmically and experimentally in support vector machines [11,12], generative adversarial network models [13,14], the solving of linear systems of equations [15–18], and the solving of linear differential equations [19]. However, principal component analysis (PCA)—one of the pioneering and most important machine learning algorithms with more than one hundred years of history [20–22]—has yet to be included in that list of areas explored. Furthermore, although the quantum PCA (qPCA) algorithm was proposed by Lloyd *et al.* in 2014 [23], it still lacks experimental demonstration. The original qPCA requires simultaneous multiple copies of a quantum state and complex quantum circuits such as quantum phase estimations, which are great challenges in an experiment.

PCA is a popular dimensionality reduction tool. It works by simplifying a semidefinite positive Hermitian matrix through decomposing it in terms of the eigenvectors with large eigenvalues [24]. On a classical computer, it is done by singular value decomposition or eigenvalue decomposition on the covariance matrix. In fact, this process can be thought of as being closely related to the hybrid classical-quantum algorithms [25–30] that aim at variational optimization with the following formulated problem. A state $\rho(\boldsymbol{\theta})$ is prepared through a quantum circuit $\mathcal{U}(\boldsymbol{\theta})$ acting on some initial state, where $\boldsymbol{\theta}$ is a vector parameterizing the quantum circuit. The expectation value of an observable $\mathrm{Tr}[\rho(\boldsymbol{\theta})P]$ is then measured as an objective function, and the parameters $\boldsymbol{\theta}$ are optimized over the objective function. In the hybrid classical-quantum algorithms, a quantum processor performs these classically daunting tasks: running the parameterized quantum circuits (PQC), evaluating the observables, and optimizing the parameters.

In this Letter, we propose a new qPCA procedure based on PQC and implement the experiments to realize the qPCA-based human face recognition on a nuclear magnetic resonance (NMR) quantum processor [12,31]. Inspired by the original qPCA by Lloyd *et al.* [23], we incorporate the hybrid classical-quantum algorithm and devise the PQC-based qPCA algorithm to be free of the multiple state copies requirement. As a verification, we conduct an experiment on the human face recognition problem, where the face images used for training and testing are all taken from the Yale Face Dataset [32]. Experimental results show that the original face images have been successfully

compressed into their corresponding eigenfaces via the qPCA implementation and that the reconstructed images from these eigenfaces recover the original faces. Now let us describe our qPCA algorithm and its experimental demonstration.

Protocol.—Given a quantum state ρ, the first step of qPCA is to find its large eigenvalues or all nonzero eigenvalues if ρ is low rank. In general, any density matrix ρ can be expanded as $\rho = \sum_{j=0}^{N-1} \lambda_j |\psi_j\rangle\langle\psi_j|$, where $\{|\psi_j\rangle\}$ is an orthogonal basis and $N = 2^n$ with n the number of qubits. Without loss of generality, we assume that the eigenvalues are sorted in descending order, i.e., $\lambda_0 \geq \lambda_1 \geq \cdots \geq \lambda_{N-1}$. If we can find a unitary operation $\mathcal{U}_g$ that maps $|\psi_j\rangle$ to $|j\rangle$, that is, diagonalizing ρ [30] as

$$\rho_f = \mathcal{U}_g \rho \mathcal{U}_g^\dagger = \sum_{j=0}^{N-1} \lambda_j |j\rangle\langle j|, \tag{1}$$

then by performing measurements in the computational basis $\{|j\rangle\}$, we are able to estimate the eigenvalue λ_j as the probability of getting $|j\rangle$. For generic states, finding such $\mathcal{U}_g$ is unlikely to be efficient. However, if ρ is highly degenerate, it is possible to do so approximately using PQC.

First, let P be a semidefinite positive and nondegenerate Hermitian operator with $|j\rangle$ the eigenstate with eigenvalue p_j, i.e., $P = \sum_{j=0}^{N-1} p_j |j\rangle\langle j|$. In contrast to the form of ρ, we assume these eigenvalues are sorted in ascending order $0 \leq p_0 < p_1 < \cdots < p_{N-1}$. In addition, we require that the operator is normalized, i.e., $\sum_j p_j = 1$. Such an operator is not hard to construct. A direct choice is a diagonal matrix with the elements $\{0, 1, 2, \ldots, N-1\}$ normalized by the factor $N(N-1)/2$. Its Pauli form is [33]

$$P = \frac{1}{N(N-1)} \sum_{j=1}^{n} 2^{j-1} (\sigma_z^j + 1), \tag{2}$$

where σ_z^j is the Pauli-Z operator acting on the jth qubit.

We claim that a unitary operator $\mathcal{U}$ that minimizes the expectation $\mathrm{Tr}(\mathcal{U}\rho\mathcal{U}^\dagger \cdot P)$ would diagonalize ρ in the computational basis, that is, make Eq. (1) hold. Here P could be an arbitrary operator as long as it meets all of the above requirements. A rigorous proof of this statement is based on the Birkhoff–von Neumann theorem [36,37] and rearrangement inequality [38] (see the Supplemental Material [33] for details). Now the problem becomes how to find $\mathcal{U}_g$. We input ρ into a PQC described by $\mathcal{U}(\boldsymbol{\theta})$ and measure the expectation value of P at the output. For instance, measuring P in Eq. (2) only requires a single Pauli-Z readout on all the qubits, which is not challenging in experiment. The objective function then reads

$$L(\boldsymbol{\theta}) = \mathrm{Tr}[\mathcal{U}(\boldsymbol{\theta}) \rho \mathcal{U}^\dagger(\boldsymbol{\theta}) \cdot P]. \tag{3}$$

By minimizing this objective function over the parameter space with some suitable optimization algorithms [33,39,40], a good approximation of $\mathcal{U}_g$ will be yielded eventually.

For many practical PCA problems, low-rank states are usually taken into account. For a PCA low-rank state ρ with the rank r, we only need to rotate the principal components of ρ into their corresponding computational basis, i.e., mapping $|\psi\rangle_{j=0}^{r}$ to $|j\rangle$, while imposing no constraints on the leftover subspace. This will significantly reduce the dimension of the search space and make it possible to find a proper $\mathcal{U}(\boldsymbol{\theta})$ with only $\sim\mathrm{poly}(n)$ free parameters. We applied this new PCA algorithm to human face recognition and verified its effectiveness experimentally.

Human face recognition.—In the following, we present the application of our qPCA algorithm on human face recognition using our qPCA algorithm, interpenetrated by the true experimental setting for better understanding. The workflow schematic for training and recognizing human faces is illustrated in Fig. 1.

We consider a training dataset containing m_1 face images and a test dataset with m_2 face images, where each image is of $M \times M$ grayscales. First, each grayscale image is reshaped into an $M^2 \times 1$ vector such that the training dataset can be described by an $M^2 \times m_1$ matrix $\boldsymbol{S} = [\boldsymbol{\nu}_1, \ldots, \boldsymbol{\nu}_{m_1}]$ and the test dataset by an $M^2 \times m_2$ matrix $\boldsymbol{X} = [\boldsymbol{\omega}_1, \ldots, \boldsymbol{\omega}_{m_2}]$. The goal is to train a PQC based on the training dataset $\boldsymbol{S}$ and then apply this trained PQC to recognize the faces in the test dataset $\boldsymbol{X}$. In experiment, we choose $m_1 = 4$ and $m_2 = 4$. Both the training and test dataset are from the Yale Face Dataset [32], and the four

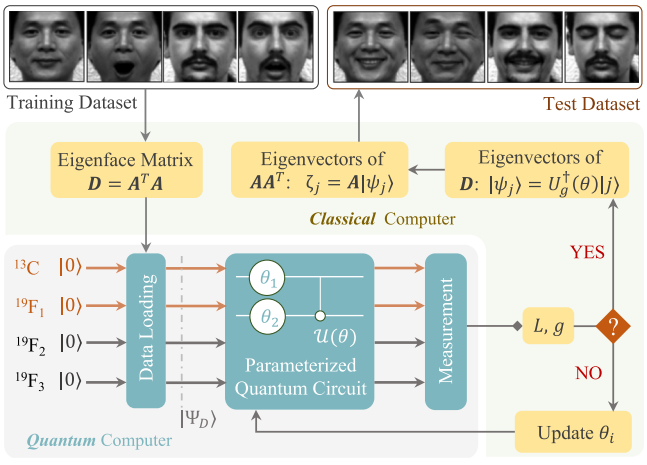

FIG. 1. Workflow for human face recognition via qPCA. The PQC $\mathcal{U}(\boldsymbol{\theta})$ is iteratively optimized via the hybrid classical-quantum control approach, where the objective function $L(\boldsymbol{\theta})$ and the gradient $g(\boldsymbol{\theta})$ are measured on the quantum processor. The storage and update of the parameters $\boldsymbol{\theta}$ are implemented on a classical computer. The optimized PQC with the operator $\mathcal{U}_g$ is applied to compute the eigenvectors of the eigenface matrix $\boldsymbol{D}$ and the covariance matrix $\boldsymbol{C} = \boldsymbol{A}\boldsymbol{A}^T$.

images in each dataset include two subjects with two facial expressions for each subject. All images are discretized by 100×100 grayscales.

Next we need to load the training dataset into the quantum circuit. This step requires an efficient implementation of quantum RAM [41,42], which is highly nontrivial in experiment. In this work, we compute a reduced $m_1 \times m_1$ (thus in experiment 4×4) matrix $\boldsymbol{D} = \boldsymbol{A}^T\boldsymbol{A}$, where $\boldsymbol{A} = \boldsymbol{S} - \bar{\boldsymbol{S}}$ and $\bar{\boldsymbol{S}} = \sum_{i=1}^{m_1} \boldsymbol{\nu}_i/m_1$. $\boldsymbol{D}$ contains the information of the so-called "eigenfaces" and actually represents some 2-qubit mixed states $\rho_{\boldsymbol{D}}$ up to normalization. To solve the eigenvectors $|\psi_j\rangle$ and eigenvalues λ_j of $\rho_{\boldsymbol{D}}$, we prepare a 4-qubit pure state $|\Psi_D\rangle$ such that after tracing out two ancillary qubits the remnant is $\rho_{\boldsymbol{D}}$. In experiment, preparing $|\Psi_D\rangle$ is a task of quantum state engineering that can be realized by gradient-based optimization [43]. This is what we have done in this experiment. For large quantum systems, potential schemes with favorable scalability also exist, such as the hybrid quantum-classical approach [40,44] combined with a direct fidelity estimation from a few Pauli measurements [45,46]. Discussions about the data loading can be found in the Supplemental Material [33].

The PQC optimization is as described in the algorithm section. The notations are the same, that is, the unitary operator of the PQC is denoted by $\mathcal{U}(\boldsymbol{\theta})$ and the measurement observable P and the objective function $L(\boldsymbol{\theta})$ have the form of Eq. (2) and Eq. (3), respectively. Here, we use the hybrid classical-quantum control method to optimize the objective function, where in each iteration $L(\boldsymbol{\theta})$ and its gradient $g(\boldsymbol{\theta})$ are measured on the quantum processor. This will remarkably enhance the precision of the trained PQC because the optimization is performed on the realistic quantum processor, incorporating some unknown errors that cannot be corrected using traditional gradient-based optimization on classical computers.

After training, an optimal parameter set $\boldsymbol{\theta}$ is found, and the PQC with the operator $\mathcal{U}_g(\boldsymbol{\theta})$ can fulfill the function of Eq. (1) with high fidelity. The eigenvalues and eigenvectors of $\rho_{\boldsymbol{D}}$ are hence $\lambda_j = \mathrm{Tr}(\rho_f|j\rangle\langle j|)$ and $|\psi_j\rangle = \mathcal{U}_g^\dagger(\boldsymbol{\theta})|j\rangle$, respectively. Note that $|\psi_j\rangle$ can be effectively computed via tensor network techniques such as the density-matrix renormalization group [47,48].

Finally, the eigenvectors of the covariance matrix, defined by $\boldsymbol{C} = \boldsymbol{A}\boldsymbol{A}^T$, are computed by $\boldsymbol{\zeta}_j = \boldsymbol{A}|\psi_j\rangle$. The covariance matrix $\boldsymbol{C}$ is the core data in PCA, which summarizes the correlations between the different components of the data. Note that the covariance matrix is an $M^2 \times M^2$ matrix (in experiment $M = 100$). The weight vectors of the training images and test images are calculated by $\Omega_j^{\mathrm{train}} = \boldsymbol{\zeta}^T(\boldsymbol{\nu}_j - \bar{\boldsymbol{S}})$ and $\Omega_j^{\mathrm{test}} = \boldsymbol{\zeta}^T(\boldsymbol{\omega}_j - \bar{\boldsymbol{S}})$, respectively. Ω^{train} and Ω^{test} can be computed with the polynomial complexity $O(m_1^2)$ [33,49]. In order to recognize a face in the test dataset, one minimizes the 2-norm $\|\Omega^{\mathrm{train}} - \Omega^{\mathrm{test}}\|$ to find which training image is closest to the test one. This completes the description of the human face recognition.

Experiment.—As described above, we need a 4-qubit quantum processor to run the qPCA-based human face recognition. The NMR system we used is the iodotrifluroethylene (C_2F_3I) molecule dissolved in d chloroform, where one ^{13}C nucleus and three ^{19}F nuclei are encoded as qubits. The internal Hamiltonian of this 4-qubit system can be written as

$$\mathcal{H}_{\mathrm{int}} = -\sum_{1\le i\le 4} \pi\nu_i\sigma_z^i + \sum_{1\le i<j\le 4} \frac{\pi}{2} J_{ij}\sigma_z^i\sigma_z^j, \tag{4}$$

where ν_i is the chemical shift of the ith spin and J_{ij} represents the coupling strength between the ith and jth spins. Each spin can be individually addressed by fast selective control pulses compared to the long coherence time of over 2.5 s measured by the Hahn echo [50]. All coupling strengths are around 300 Hz, so 2-qubit gates can be realized in less than 2 ms. More properties and parameters about the molecule can be found in the Supplemental Material [33]. Experiments are carried out at 298 K on a Bruker 600 MHz spectrometer.

The implemented circuit is presented in Fig. 1. In experiment, we first create the $|\mathbf{0}\rangle \equiv |0\rangle^{\otimes 4}$ pseudo-pure state via the selective-transition method [51]. Its fidelity is over 99% via 4-qubit quantum state tomography [33], which sets up a reliable ground for subsequent experiments. To initialize the eigenface density matrix $\rho_{\boldsymbol{D}}$ of the training dataset, we apply a shaped pulse optimized by the well-established NMR control techniques to prepare a 4-qubit pure state $|\Psi_D\rangle$, whose form is exactly $\rho_{\boldsymbol{D}}$ after tracing out two ancillary qubits [33].

The experimental PQC contains two layers. In each layer, the unitary evolution is $\prod_{i=1}^{n-1} \mathrm{CNOT}_{i,i+1} \prod_{i=1}^{n} R_y^i(\theta_i)$, where $n = 2$ is the number of work qubits, $\mathrm{CNOT}_{i,i+1}$ represents a controlled-NOT gate of control qubit i and target qubit $i+1$, and $R_y^i(\theta_i)$ represents a θ_i single-qubit rotation about the y axis. In experiment, the single-qubit rotations and CNOT gates are realized by 0.5 ms and 2.5 ms pulses of over 0.995 fidelities, respectively. Hence, the 2-layer PQC $\mathcal{U}(\boldsymbol{\theta})$ contains four rotating angles to be optimized, i.e., the parameter $\boldsymbol{\theta}$ can be written as a row vector $\{\theta_j, 1 \le j \le 4\}$. The optimization is implemented via the hybrid classical-quantum control approach as follows.

We start from an initial guess $\boldsymbol{\theta}^{(1)}$, where the superscript (1) denotes the iteration number. We perform the PQC $\mathcal{U}[\boldsymbol{\theta}^{(1)}]$ and measure the objective function $L[\boldsymbol{\theta}^{(1)}]$. As defined in Eq. (2), the experimental P is chosen as $P = (\sigma_z^1 + 2\sigma_z^2 + 3\mathbb{I})/12$, which has a positive, normalized, and nondegenerate energy spectrum. In the NMR experiment, $\langle\sigma_z^1\rangle$ is directly measured by flipping the first spin ^{13}C, and $\langle\sigma_z^2\rangle$ is measured by transferring its signal to the first spin using a SWAP_{12} gate [33].

To update the parameter $\boldsymbol{\theta}$, we need to measure the gradient $g(\boldsymbol{\theta}) = \nabla L(\boldsymbol{\theta})$. In experiment, we adopt the $\pm\pi/2$-method to measure the gradient for each θ_j. For example, in

the kth iteration, we increase and decrease each $\theta_j^{(k)}$ $(1 \le j \le 4)$ by $\pi/2$, measure the corresponding objective functions, and calculate the gradient by [33]

$$g[\theta_j^{(k)}] = \frac{1}{2}\left\{ L\left[\boldsymbol{\theta}^{(k)} : \theta_j^{(k)} + \frac{\pi}{2}\right] - L\left[\boldsymbol{\theta}^{(k)} : \theta_j^{(k)} - \frac{\pi}{2}\right]\right\}. \quad (5)$$

For the $(k+1)$th iteration, the parameter is updated by $\boldsymbol{\theta}^{(k+1)} = \boldsymbol{\theta}^{(k)} - \alpha^{(k)} \cdot \boldsymbol{g}[\theta^{(k)}]$, where $\alpha^{(k)}$ is the step size in the gradient-based optimization. This optimization is repeated until L converges to the minimal value. We can see that this optimization is implemented on the quantum processor, so it can incorporate some unknown errors occurring in the processor, which are hard to take into account in a pure classical optimization process. As a result, after 10 iterations, the objective function L decreases to very close to the global minimum as shown in Fig. 2(a).

Results.—We also perform quantum state tomography [33] on the work qubits and calculate the fidelities of the reconstructed density matrices $\rho[\boldsymbol{\theta}^{(k)}]$ compared to the numerically simulated ones via $F(\rho,\sigma) = \mathrm{Tr}(\rho\sigma)/\sqrt{\mathrm{Tr}(\rho^2)\mathrm{Tr}(\sigma^2)}$, as shown in the inset of Fig. 2(a). The fidelity increases to 99.06% after 10 iterations. Moreover, we compute the eigenvector $|\psi_j\rangle^{(k)} = \mathcal{U}^\dagger(\boldsymbol{\theta}^{(k)})|j\rangle$ at each iteration, where $|j\rangle$ is the jth eigenvector of P in the ascending order. Figure 2(b) presents the similarity of $|\psi_j\rangle^{(k)}$ with the ideal eigenvector of the eigenface matrix $\boldsymbol{D}$, defined by the distance function $\mathcal{D}(\boldsymbol{a},\boldsymbol{b}) = |\boldsymbol{a}\cdot\boldsymbol{b}|/|\boldsymbol{a}|^2|\boldsymbol{b}|^2$. The corresponding eigenvalues as a function of iteration number k are plotted in Fig. 2(c). These values are eventually very close to those of the eigenface matrix $\boldsymbol{D}$. Therefore, 10 iterations on a quantum processor successfully accomplishes the optimization process to get the eigenvalues and eigenvectors of the eigenface matrix $\boldsymbol{D}$.

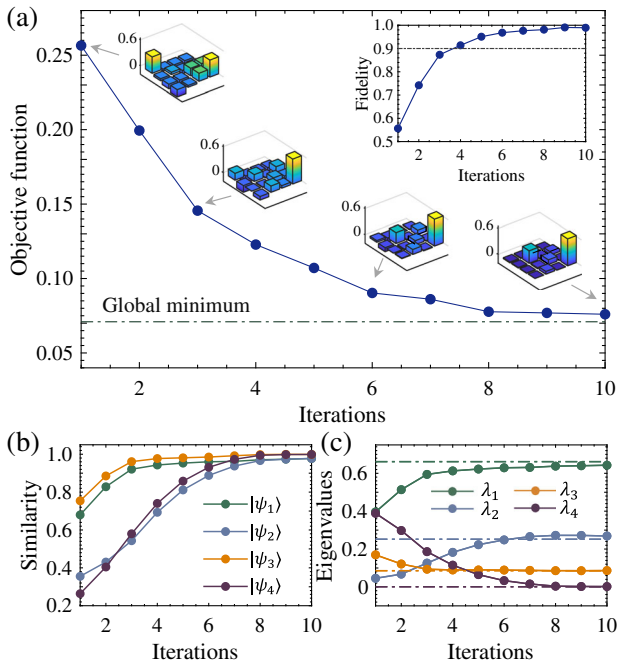

FIG. 2. Experimental results of hybrid classical-quantum optimization. (a) Value of objective function $L[\boldsymbol{\theta}^{(k)}]$ as a function of the iteration k. Inset is the fidelity curve of the instantaneous density matrix $\rho[\boldsymbol{\theta}^{(k)}]$ compared to the simulated one. Some bar forms of the density matrices are also plotted along with the objective function curve. (b) Similarity of the eigenvectors $|\psi_j\rangle^{(k)}$ compared to the ideal ones of the eigenface matrix $\boldsymbol{D}$. (c) Eigenvalues $\lambda_j^{(k)}$ as a function of the iteration k and the theoretical eigenvalues of $\boldsymbol{D}$ are represented by the dotted horizontal lines.

To recognize the human faces in the test dataset, we compute the eigenvectors of the covariance matrix $\boldsymbol{C}$ by $\boldsymbol{\zeta}_j = \boldsymbol{A}|\psi_j\rangle$. This gives the eigenface images from the training dataset, as shown in the left column of Fig. 3. For each of the four test images, we compute its weight vector $\Omega_j^{\mathrm{test}} = \boldsymbol{\zeta}^T(\boldsymbol{\omega}_j - \bar{\boldsymbol{S}})$ and compare it to the weight vectors of the training dataset $\Omega_j^{\mathrm{train}} = \boldsymbol{\zeta}^T(\boldsymbol{\nu}_j - \bar{\boldsymbol{S}})$. This comparison is encoded by the 2-norm $\|\Omega^{\mathrm{train}} - \Omega^{\mathrm{test}}\|$, and the experimental values are listed in the table in Fig. 3. It is obvious that each test image, despite the distinct facial expressions, can be successfully recognized to be the right subject from its 2-norm values.

As an extension, we also simulate this qPCA method in processing image recognition problems with a larger dataset using different types of PQCs [27,52] to study how to design PQCs and compare their performances in terms of the nearest-neighbor, circuit-block, and all-to-all connectivity in qubits, respectively. Figure 4 gives an example of training 16 face images in an all-to-all connected PQC. The number of layers needs to be carefully determined, accounting for factors that include the expressibility of quantum circuits, the number of optimized parameters, and

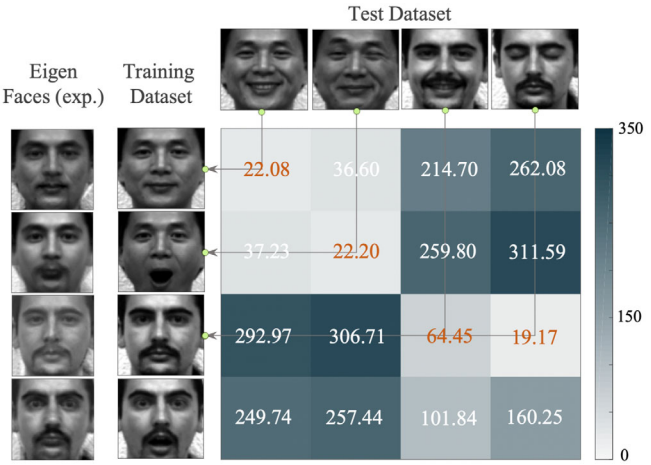

FIG. 3. Human face recognition results from the test dataset. The 2-norm $\|\Omega^{\mathrm{train}} - \Omega^{\mathrm{test}}\|$ values are calculated for each test image compared to all training images, as listed in the table, while the least 2-norm value indicates the recognition result. Experimental eigenface images of the training dataset using the qPCA approach are plotted in the left column.

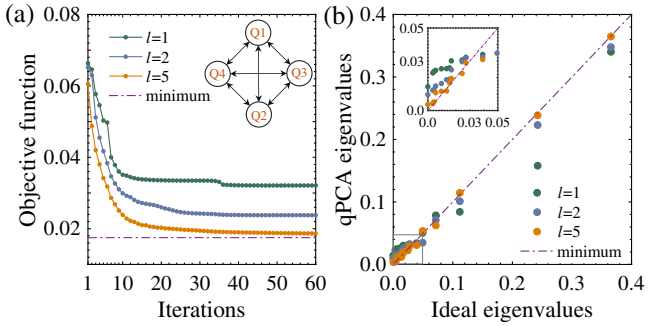

FIG. 4. Numerical results for tackling image recognition problems with 16 face images. The PQC is chosen to be an all-to-all connected one, $U_l^{\mathrm{AA}}(\theta) = \prod_{p=1}^{4}\prod_{j=1,\neq p}^{4}\mathrm{CNOT}_{p,j}\prod_{i=1}^{n}R_y^i(\theta_i^{l,p})$. (a) Convergence of the objective function using the PQC with l layers. (b) Optimized eigenvalues shown in comparison to the ideal ones at each iteration for PQC with different layers.

the training cost. We discuss in detail this determination by numerical simulation in the Supplemental Material [33].

Conclusion.—As a popular tool in many machine learning tasks, classical PCA suffers a severe scaling problem when computing the eigenvalues and eigenvectors of the covariance matrix. Rather than use the original qPCA algorithm that requires multiple copies of quantum states and the implementation of quantum phase estimations, we propose a new qPCA approach based on the hybrid classical-quantum control. By optimizing the multilayer PQC with an appropriate measuring observable, the eigenvalues and eigenvectors can be efficiently obtained with the aid of a quantum processor. We apply our qPCA method to a human face recognition problem with four images in the training dataset and four images in the test dataset. By training a 4-qubit NMR quantum processor, the eigenfaces of the training images are extracted with high fidelities, and all test images are recognized correctly. As an efficient way of loading classical data into quantum states is not yet realized in any experiment, our proof-of-principle demonstration cannot offer a quantum speedup. However, once some quantum RAM architecture, e.g., the "bucket brigade" approach [41,42] or others, can be efficiently implemented in experiment, the proposed qPCA algorithm promises more applications in machine learning tasks.

This work is supported by the National Key Research and Development Program of China (2019YFA0308100), the National Natural Science Foundation of China (12075110, 11975117, 11905099, 11875159, and U1801661), the Guangdong Basic and Applied Basic Research Foundation (2019A1515011383), the Guangdong International Collaboration Program (2020A0505100001), the Science, Technology and Innovation Commission of Shenzhen Municipality (ZDSYS20170303165926217, KQTD2019 0929173815000, JCYJ20200109140803865, JCYJ20170 412152620376, and JCYJ20180302174036418), the Pengcheng Scholars, the Guangdong Innovative and Entrepreneurial Research Team Program (2019ZT08C044), and the Guangdong Provincial Key Laboratory (2019B12 1203002). Y. D. is supported by the Major Scientific Research Project of Zhejiang Lab (2019 MB0AD01).

T. X. and L. C. contributed equally to this work.

*Corresponding author.
xint@sustech.edu.cn
†Corresponding author.
lij3@sustech.edu.cn
‡Corresponding author.
yingdong@zhejianglab.edu.cn
§Corresponding author.
ludw@sustech.edu.cn

[1] G. Carleo, I. Cirac, K. Cranmer, L. Daudet, M. Schuld, N. Tishby, L. Vogt-Maranto, and L. Zdeborová, Rev. Mod. Phys. **91**, 045002 (2019).
[2] J. Biamonte, P. Wittek, N. Pancotti, P. Rebentrost, N. Wiebe, and S. Lloyd, Nature (London) **549**, 195 (2017).
[3] V. Dunjko, J. M. Taylor, and H. J. Briegel, Phys. Rev. Lett. **117**, 130501 (2016).
[4] J. Carrasquilla and R. G. Melko, Nat. Phys. **13**, 431 (2017).
[5] G. Carleo and M. Troyer, Science **355**, 602 (2017).
[6] M. Broughton, G. Verdon, T. McCourt, A. J. Martinez, J. H. Yoo, S. V. Isakov, P. Massey, M. Y. Niu, R. Halavati, E. Peters *et al.*, arXiv:2003.02989.
[7] I. Cong, S. Choi, and M. D. Lukin, Nat. Phys. **15**, 1273 (2019).
[8] M. H. Amin, E. Andriyash, J. Rolfe, B. Kulchytskyy, and R. Melko, Phys. Rev. X **8**, 021050 (2018).
[9] M. Benedetti, E. Lloyd, S. Sack, and M. Fiorentini, Quantum Sci. Technol. **4**, 043001 (2019).
[10] J. Romero, J. P. Olson, and A. Aspuru-Guzik, Quantum Sci. Technol. **2**, 045001 (2017).
[11] P. Rebentrost, M. Mohseni, and S. Lloyd, Phys. Rev. Lett. **113**, 130503 (2014).
[12] Z. Li, X. Liu, N. Xu, and J. Du, Phys. Rev. Lett. **114**, 140504 (2015).
[13] S. Lloyd and C. Weedbrook, Phys. Rev. Lett. **121**, 040502 (2018).
[14] L. Hu, S.-H. Wu, W. Cai, Y. Ma, X. Mu, Y. Xu, H. Wang, Y. Song, D.-L. Deng, C.-L. Zou *et al.*, Sci. Adv. **5**, eaav2761 (2019).
[15] A. W. Harrow, A. Hassidim, and S. Lloyd, Phys. Rev. Lett. **103**, 150502 (2009).
[16] Y. Zheng, C. Song, M.-C. Chen, B. Xia, W. Liu, Q. Guo, L. Zhang, D. Xu, H. Deng, K. Huang, Y. Wu, Z. Yan, D. Zheng, L. Lu, J.-W. Pan, H. Wang, C.-Y. Lu, and X. Zhu, Phys. Rev. Lett. **118**, 210504 (2017).
[17] X.-D. Cai, C. Weedbrook, Z.-E. Su, M.-C. Chen, M. Gu, M.-J. Zhu, L. Li, N.-L. Liu, C.-Y. Lu, and J.-W. Pan, Phys. Rev. Lett. **110**, 230501 (2013).
[18] J. Pan, Y. Cao, X. Yao, Z. Li, C. Ju, H. Chen, X. Peng, S. Kais, and J. Du, Phys. Rev. A **89**, 022313 (2014).
[19] T. Xin, S. Wei, J. Cui, J. Xiao, I. n. Arrazola, L. Lamata, X. Kong, D. Lu, E. Solano, and G. Long, Phys. Rev. A **101**, 032307 (2020).
[20] T. Fukushima, J. Anthropol. Soc. Nippon **75**, 69 (1967).

[21] P. Baldi and K. Hornik, Neural Netw. **2**, 53 (1989).
[22] C. Ding and X. He, in *Proceedings of the Twenty-First International Conference on Machine Learning* (2004), p. 29.
[23] S. Lloyd, M. Mohseni, and P. Rebentrost, Nat. Phys. **10**, 631 (2014).
[24] S. Rajendran, A. Kaul, R. Nath, A. Arora, and S. Chauhan, in *2014 International Conference on Signal Propagation and Computer Technology (ICSPCT 2014)* (IEEE, 2014), pp. 561–566.
[25] J. R. McClean, J. Romero, R. Babbush, and A. Aspuru-Guzik, New J. Phys. **18**, 023023 (2016).
[26] T. Xin, X. Nie, X. Kong, J. Wen, D. Lu, and J. Li, Phys. Rev. Applied **13**, 024013 (2020).
[27] T. Hubregtsen, J. Pichlmeier, and K. Bertels, arXiv:2003.09887.
[28] A. Peruzzo, J. McClean, P. Shadbolt, M.-H. Yung, X.-Q. Zhou, P. J. Love, A. Aspuru-Guzik, and J. L. O'brien, Nat. Commun. **5**, 4213 (2014).
[29] J. Tangpanitanon, S. Thanasilp, N. Dangniam, M.-A. Lemonde, and D. G. Angelakis, arXiv:2005.11222.
[30] R. LaRose, A. Tikku, É. O'Neel-Judy, L. Cincio, and P. J. Coles, npj Quantum Inf. **5**, 57 (2019).
[31] X.-W. Yao, H. Wang, Z. Liao, M.-C. Chen, J. Pan, J. Li, K. Zhang, X. Lin, Z. Wang, Z. Luo, W. Zheng, J. Li, M. Zhao, X. Peng, and D. Suter, Phys. Rev. X **7**, 031041 (2017).
[32] Yale Face Database, http://cvc.cs.yale.edu/cvc/.
[33] See Supplemental Material, which includes Refs. [34,35], at http://link.aps.org/supplemental/10.1103/PhysRevLett.126.110502 for a complete description of the qPCA algorithm, experimental details, and numerical simulations.
[34] K. Pearson, Lond. Edinburgh Dublin Philos. Mag. J. Sci. **6**, 559 (1901).
[35] M. K. Kozlov, S. P. Tarasov, and L. G. Khachiyan, in *Doklady Akademii Nauk*, Vol. 248 (Russian Academy of Sciences, 1979), pp. 1049–1051.
[36] G. Birkhoff, Rev. Ser. A **5**, 147 (1946).
[37] J. Von Neumann, Contrib. Theory Games **2**, 5 (1953).
[38] G. H. Hardy, J. E. Littlewood, G. Pólya, G. Pólya, D. Littlewood *et al.*, *Inequalities* (Cambridge University Press, Cambridge, England, 1952).
[39] R. Sweke, F. Wilde, J. Meyer, M. Schuld, P. K. Fährmann, B. Meynard-Piganeau, and J. Eisert, Phys. Rev. Research **2**, 043364 (2020).
[40] J. Li, X. Yang, X. Peng, and C.-P. Sun, Phys. Rev. Lett. **118**, 150503 (2017).
[41] V. Giovannetti, S. Lloyd, and L. Maccone, Phys. Rev. Lett. **100**, 160501 (2008).
[42] C. Ciliberto, M. Herbster, A. D. Ialongo, M. Pontil, A. Rocchetto, S. Severini, and L. Wossnig, Proc. R. Soc. A **474**, 20170551 (2018).
[43] N. Khaneja, T. Reiss, C. Kehlet, T. Schulte-Herbrüggen, and S. J. Glaser, J. Magn. Reson. **172**, 296 (2005).
[44] D. Lu, K. Li, J. Li, H. Katiyar, A. J. Park, G. Feng, T. Xin, H. Li, G. Long, A. Brodutch *et al.*, npj Quantum Inf. **3**, 45 (2017).
[45] S. T. Flammia and Y.-K. Liu, Phys. Rev. Lett. **106**, 230501 (2011).
[46] M. P. da Silva, O. Landon-Cardinal, and D. Poulin, Phys. Rev. Lett. **107**, 210404 (2011).
[47] S. R. White and A. E. Feiguin, Phys. Rev. Lett. **93**, 076401 (2004).
[48] U. Schollwöck, Rev. Mod. Phys. **77**, 259 (2005).
[49] S. S. Skiena, in *The Algorithm Design Manual* (Springer, New York, 2012), pp. 103–144.
[50] E. L. Hahn, Phys. Rev. **80**, 580 (1950).
[51] X. Peng, X. Zhu, X. Fang, M. Feng, K. Gao, X. Yang, and M. Liu, Chem. Phys. Lett. **340**, 509 (2001).
[52] S. Sim, P. D. Johnson, and A. Aspuru-Guzik, Adv. Quantum Technol. **2**, 1900070 (2019).